Lanthanide Identity Governs Guest-Induced Dimerization in $Ln^{III}[15\text{-}MC_{Cu^{II}N(L\text{-}pheHA)}\text{-}5])^{3+}$ Metallacrowns

Carmelo Sgarlata[+],*[a] Bernadette L. Schneider[+],[b] Valeria Zito,[d] Rossella Migliore,[a] Matteo Tegoni,*[c] Vincent L. Pecoraro,*[b] and Giuseppe Arena*[a]

Abstract: Series of lanthanide-containing metallic coordination complexes are frequently presented as structurally analogous, due to the similar chemical and coordinative properties of the lanthanides. In the case of chiral $(Ln^{III}[15\text{-}MC_{Cu^{II}N(L\text{-}pheHA)}\text{-}5])^{3+}$ metallacrowns (MCs), which are well established supramolecular hosts, the formation of dimers templated by a dicarboxylate guest (muconate) in solution of neutral pH is herein shown to have a unique dependence on the identity of the MC's central lanthanide. Calorimetric data and nuclear magnetic resonance diffusion studies demonstrate that MCs containing larger or smaller lanthanides as the central metal only form monomeric host-guest complexes whereas analogues with intermediate lanthanides (for example, Eu, Gd, Dy) participate in formation of dimeric host-guest-host compartments. The driving force for the dimerization event across the series is thought to be a competition between formation of highly stable MCs (larger lanthanides) and optimally linked bridging guests (smaller lanthanides).

Introduction

Synthetic supramolecular complexes with a hydrophobic cavity are attractive for their likeness to the hydrophobic active sites of some enzymes, which are highly substrate-selective through a combination of appropriate chemical interactions balanced with suitable shape and size. Along this vein, supramolecular complexes may take the approach of utilizing the steric and chemical conditions of such a hydrophobic compartment to enhance host-guest selectivity, including several examples of metal-based supramolecular catalysts.[1] Understanding the non-covalent interactions that drive formation of molecular nano-compartments in solution is critical for development of the function and applications of such systems.

Metallacrowns (MCs), a class of metallamacrocycles that are structurally analogous to crown ethers, self-assemble typically from hydroximate ligands and transition metal ions to form an [M–N–O] repeating unit in place of the more familiar [C–C–O] repeat of crown ethers.[2] Within the subgroup known as 15-metallacrown-5 (15-MC-5), the incorporation of chiral *L*-phenylalanine hydroximate (pheHA) ligands with Cu^{2+} and a central lanthanide coordinated by the oxime oxygens creates a "hand-like" amphipathic metallacrown with a hydrophilic face and an opposing hydrophobic face, which is capable of selectively recognizing various moieties, such as nitrates, carboxylates, and chiral amino acids.[3] Crystallographically, we observed these MC-guest complexes were capable of selectively sequestering dicarboxylate guests of appropriate size within the hydrophobic interior cavity of an MC dimer (Scheme 1).[4] Our recent investigation of the behavior of metallacrown-dicarboxylate

[a] *Prof. C. Sgarlata,[+] Dr. R. Migliore, Prof. G. Arena*
Dipartimento di Scienze Chimiche
Università degli Studi di Catania
Viale Andrea Doria 6, 95125 Catania (Italy)
E-mail: sgarlata@unict.it
garena@unict.it
[b] *B. L. Schneider,[+] Prof. V. L. Pecoraro*
Department of Chemistry
University of Michigan
Ann Arbor, MI 48109 (USA)
E-mail: vlpec@umich.edu
[c] *Prof. M. Tegoni*
Department of Chemistry
Life Sciences and Environmental Sustainability
University of Parma
Parco Area delle Scienze 17 A, 43124, Parma (Italy)
E-mail: matteo.tegoni@unipr.it
[d] *V. Zito*
Institute of Crystallography
National Research Council (CNR), S.S. Catania
Via P. Gaifami 18, 95126 Catania (Italy)
[+] *These authors contributed equally to this manuscript.*
Supporting information for this article is available on the WWW under https://doi.org/10.1002/chem.202103263

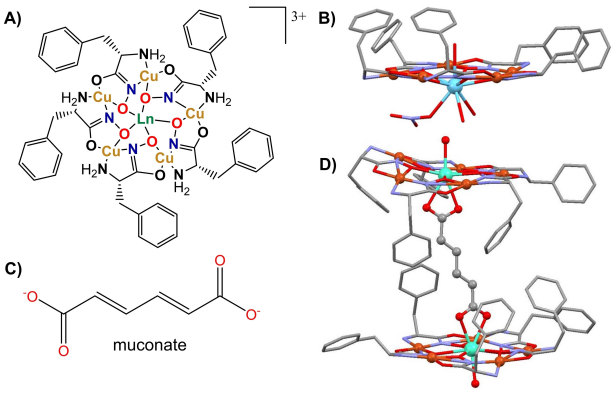

Scheme 1. Illustrations of $(Ln^{III}[15\text{-}MC_{Cu^{II}N(L\text{-}pheHA)}\text{-}5])^{3+}$ (A and B),[4a] dicarboxylate guest (C), and host-guest-host dimeric compartment (D).[4c]

systems in aqueous solution demonstrated that (Gd^{III}[15-$MC_{Cu^{II}N(L\text{-}pheHA)}$-5])$^{3+}$ (**Gd-MC**) could form a dimeric 2:1 MC_2-guest complex at neutral pH that remained in equilibrium with a 1:1 MC-guest complex.[5] Further evaluation of the solution behavior of this system when different lanthanides occupy the central MC cavity is warranted.

Structurally, lanthanides frequently are treated as interchangeable – often existing as 3+ cations (at neutral pH and ambient temperatures) with similar coordination geometries that lead to the ability to synthesize a series of structurally analogous compounds varying only by identity of the lanthanide. However, the trivalent lanthanides decrease in radius by almost 0.2 Å across the series (1.16 Å (La^{3+}) to 0.98 Å (Lu^{3+}) for eight-coordinate ions) and increase in radius with greater coordination number (for La^{3+}, radius increases from 1.10 Å to 1.27 Å for coordination number 7 to 10)[6] which can lead to slight differences in structure and stability. Within the series of isostructural 15-MC-5 pheHA-based metallacrowns, as the lanthanide ion radius increases, the diameter of the MC ring cavity expands to accommodate the larger ions, with a corresponding increase in planarity of the MC ring[7] and reduced thermodynamic stability of the complex with respect to Ln coordination in the central cavity.[8] Therefore, we wished to examine implications of different lanthanides for the solution-state formation of the MC_2 dimer, expecting small to moderate differences in the thermodynamic parameters, when compared to the previously published **Gd-MC**. Much to our surprise, we observed that with certain lanthanides, the 15-MC-5 metallacrowns were completely unable to participate in guest-induced dimerization. We present our results examining this effect by two complementary techniques: calorimetry and NMR.

Results and Discussion

Calorimetry

Since calorimetry has been shown to be an accurate and reliable technique to determine both the species and their binding constants in solution[3b,5,9] we resorted to Isothermal Titration Calorimetry (ITC), as done previously with **Gd-MC**.[5] Also, since it was proved that the chain length is the crucial parameter for the formation of the compartment in solution, we focused our attention on the interaction of muconate (Muc) with a series of (Ln^{III}[15-$MC_{Cu^{II}N(L\text{-}pheHA)}$-5])$^{3+}$ (Ln = La, Nd, Sm, Eu, Dy, Ho) metallacrowns to assess whether the central ion of the cavity affected the formation of the complex species in solution. The power curves for the **Eu-MC**/, **Sm-MC**/, **Nd-MC**/Muc and blank dilution systems are reported in Figures S1–S4 (see Supporting Information) as an example. As we titrate the guest into the **Ln-MC**, the formation of the 2:1 (**MC**-guest-**MC**) compartment is more favored in the earliest region at very low guest/host ratio. To analyze this region, we had to expand the very initial region of the full scan titration since the initial points of a power curve unfortunately suffer from the so called 'first injection anomaly';[10] thus, if we were to exclude the first one-two points from a full scan titration, we would neglect the entire set of points collected with an 'expanded' titration. On the other hand, such a procedure, while permitting collection of a sufficient number of points in the region of interest, poses a problem since the software provided by ITC manufacturers does not provide capability for the combined refinement of different titrations. The inset of Figure S1, S2, or S3 shows a titration that expands the very first region of the full scan curve. To refine full scan and expanded titrations together we used HypCal,[11] a software, set up *ad hoc* in our research group, that allows for the simultaneous refinement of calorimetric data collected from different titrations. Experiments were designed so that full scan and expanded titrations would have comparable power values; this avoids weighting data points (or titrations) which might introduce artifacts. 1:1 and 2:1 species were tested both separately and in combination and led to the results summarized in Figure 1 as well as in Table S1.

Despite numerous attempts (change of Muc/**Ln-MC** ratios and concentrations), some **Ln-MC**s unvaryingly failed to show the formation of the **MC**-guest-**MC** species (Figure 1). **Ho-MC** represents a case of its own. Although there were indications of formation of the 2:1 (**Ho-MC**)$_2$-Muc species, its percentage was so low as to hamper a satisfactory determination; in other

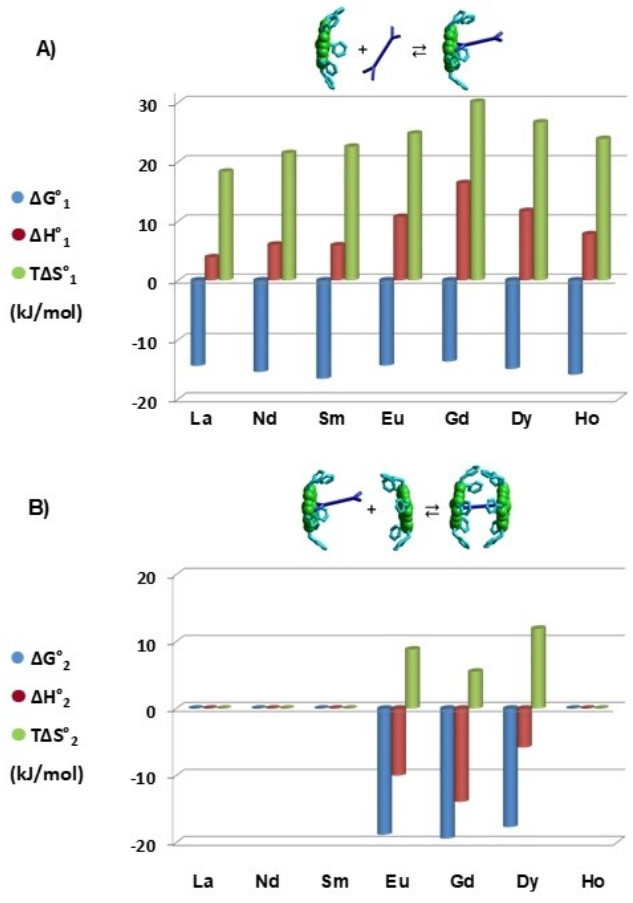

Figure 1. Thermodynamic parameters for the species obtained by titrating muconate solution into a solution of **Ln-MC** host, for each of the **Ln-MC**s examined, at 25 °C in buffered aqueous solution (pH 7.2, 50 mM MOPS).

words, its exclusion did not alter significantly the statistical parameters, that are used as a criterion to accept/reject a model.

The first inclusion step is entropically favored and driven for all **Ln-MC**s, regardless of whether or not the process goes any further to yield the (**Ln-MC**)$_2$Muc species, and this indicates that the inclusion of muconate into the **MC** cavity involves a significant desolvation. A (**Ln-MC**)$_2$Muc species is detected for Eu, Gd, and Dy only. Unlike for the formation of (**Ln-MC**)Muc, for this second step (that is, the formation of a compartment), the enthalpic contribution is always favorable whilst the entropic contribution is significantly lower than that determined for the first step. This indicates that (i) the entropy gained when desolvation of an **MC** is induced by a system (**Ln-MC**)Muc that has already desolvated is sizably smaller than when induced by a free guest (Muc) and (ii) the compartment involves additional intramolecular (favorable) interactions that are not present in the 1:1 species. This may be explained by assuming that in solution the (**Ln-MC**)$_2$Muc species maintains the arrangement found in the solid state in which the phenyl substituents of the metallacrown contact one another like two folded hands forming a compartment that incorporates the dicarboxylate allowing the phenyl groups from the two metallacrown units to give rise to a favorable π-π interaction[4] (Scheme 1D). In summary, the lower entropic contribution of the second step would result from a lesser desolvation as well as from the formation of a more rigidified ensemble.

In any case the ΔG° value of the second step for the three **Ln-MC** systems in which the formation of a compartment is detected is always larger than that of the first step. Interestingly, such a trend had already been found for compartments formed by **Gd-MC** with a series of dicarboxylates, including muconate, in a previous work[5] and is here observed again for both the Eu and Dy (**Ln-MC**)$_2$Muc species. This further corroborates the interpretation of the thermodynamic data as it shows that in this step there is a degree of cooperativity (that is, an extra-stabilization with respect to the first step) that ranges from 3–4 kJ mol^{-1} for the Eu and Dy species to about 6 kJ mol^{-1} for the Gd system.

Pulsed-gradient diffusion ordered NMR

Despite line broadening of NMR signals due to the presence of Cu^{2+} in the metallacrown ring and Ln^{3+} in the central cavity, we are able to collect paramagnetic ^{1}H NMR spectra for several species of the $(Ln^{III}[15\text{-}MC_{Cu^{II}N(L\text{-}pheHA)}\text{-}5])^{3+}$ series (La, Nd, Sm, Eu, Tb, Dy, Ho, Er) and Y^{3+} (Figure S5). Inversion recovery experiments determined the T_1 (longitudinal) relaxation time for each proton in the complex (Table S2). When subjected to the gradient sequence of the diffusion ordered spectroscopy experiment (DOSY), proton relaxation in Y and La complexes (although these have diamagnetic central metals) was too attenuated for collection of PGSE NMR. Based on experience with other paramagnetic MC systems,[12] we attribute the sharpening of spectral lines for certain **Ln-MCs** (for example, with paramagnetic central metals such as Nd or Sm) to additional coupling between the central paramagnetic lanthanide and the copper(II) coupled system. According to relaxation rate principles,[13] the coupling between a fast relaxing and a slow relaxing metal results in the increase of the electron relaxation rate of the slowest, which in turn slows down the relaxation of the nearby ^{1}H nuclei.[12] We determined that three of the species with the longest relaxation times (Nd, Sm, Eu) were suitable for study with a pulsed gradient spin echo (PGSE) NMR sequence. We were only able to collect data for one species (**Eu-MC**) that was shown by ITC to participate in formation of the (**Ln-MC**)$_2$Muc species, since the very fast relaxation times of **Dy-MC** and **Gd-MC** species proved unsuitable for analysis using our pulsed gradient sequence.

In the host-guest equilibrium of the **Ln-MC**-carboxylate system, the observed value of D depends on the coefficients D_{MC}, $D_{1:1}$, and $D_{2:1}$, where MC, 1:1, and 2:1 refer to free MC, 1:1 (**Ln-MC**)Muc adduct, and 2:1 the dimeric (**Ln-MC**)$_2$Muc capsule, respectively. The observed D depends also on the relative amount of each species in solution, in turn depending on the formation constants and molar fractions (χ) of the different species (Eq. 1):

$$D_{obs} = D_{MC}\chi_{MC} + D_{1:1}\chi_{1:1} + D_{2:1}\chi_{2:1} \quad (1)$$

In the presence of the internal standard DMSO, however, it is convenient to use the following (Eq. 2):

$$D'_{obs} = (D'_{MC} \cdot \%_{MC} + D'_{1:1} \cdot \%_{1:1} + D'_{2:1} \cdot \%_{2:1}) \cdot \frac{1}{100} \quad (2)$$

where the D' values of MC, 1:1 and 2:1 species correspond to $\frac{D_{species}}{D_{DMSO}}$. D'_{obs} is $\frac{D_{obs}}{D_{DMSO}}$ which equals the ratio of the exponential decay parameters of the MC and DMSO in the PGSE experiment at the titration point at which the % values of the species are calculated,that is, from the formation constants of the **Ln-MC**/muconate adducts obtained using speciation information obtained by calorimetry (speciation diagrams shown as Figures S6–S9). As described by Stokes-Einstein theory, the decrease of D_{obs} (and consequently of $\frac{D_{obs}}{D_{DMSO}}$) can be attributed to an increase in the size of the MC over the course of the titration.[14]

The D'_{obs} values for the **Eu-MC**, **Nd-MC**, and **Sm-MC** over the course of titration with potassium muconate as dicarboxylate guest as well as titration of **Eu-MC** with potassium sorbate, as monocarboxylate, are presented in Figure 2 as an average of 3 titrations. Minimal change in diffusion is observed for titrations of **Sm-MC** and **Nd-MC** with Muc (~2%), but a more significant decrease is observed for the **Eu-MC**/Muc system (~8%). Precipitation of the complex occurred at titration points beyond the highest MC concentrations shown. A control titration with potassium sorbate as guest with **Eu-MC** indicates that a monocarboxylate does not induce a change in the diffusion and that the observed decrease with the dicarboxylate is a valid effect. Simple ^{1}H NMR for this titration shows changes in chemical shift for both the MC and sorbate, implying an interaction between the two species is maintained (Figure S10). As compared to the NMR spectra of **Sm-MC** and **Nd-MC**, the observed signal for the **Eu-MC** was less intense due to its

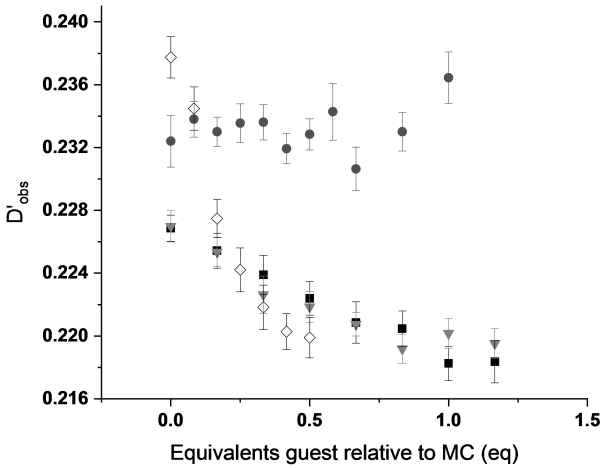

Figure 2. Change in diffusion coefficient of the Ln^{III}[15-$MC_{Cu\ N(L\text{-}pheHA)}$-5])$^{3+}$ species, characterized by $D'_{obs} = D_{obs}/D_{DMSO}$ as it is titrated with muconate or sorbate guest as determined by NMR. Black squares: **Nd-MC** (2 mM) with 40 mM Muc; gray triangles: **Sm-MC** (2 mM) with 40 mM Muc; open diamonds: **Eu-MC** (6 mM) with 60 mM Muc; dark gray circles **Eu-MC** (6 mM) with 60 mM sorbate. Each point was calculated as the ratio of the exponential decay parameters determined by fit of combined data of multiple PGSE ^{1}H NMR experiments. **Eu-MC**/Muc titration at 6 mM resulted in significant precipitation after 0.5 equiv. muconate added.

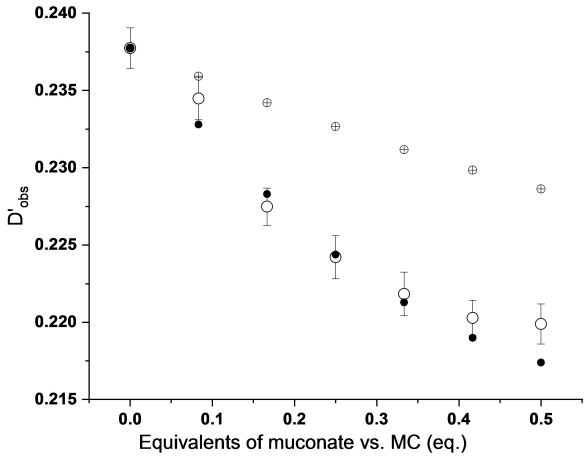

Figure 3. Regression analysis of the NMR titration of **Eu-MC** with muconate. Open circles: observed D'_{obs} values for the titration of **Eu-MC** with up to 0.5 equiv. of muconate. Black dots: calculated D′ at the points of the titration using the speciation of **Eu-MC** provided by calorimetric data (2:1 species present in the speciation). Crossed circles: calculated D' at the points of the titration using the speciation of **Sm-MC** provided by calorimetric data (2:1 species not present in the speciation).

shorter T_1. This decreased sensitivity required more concentrated samples (6 mM, as opposed to 2 mM) as well as adjustment of experimental parameters, in which a very short relaxation delay parameter was employed.

To evaluate reliability of the NMR and test whether ITC and NMR data reinforce one another, Equation (2) was used to determine D'_{MC}, $D'_{1:1}$, and $D'_{2:1}$ coefficients by least square fit of the D'_{obs} values obtained from the muconate titrations with % values from ITC used as fixed parameters in the least square analysis. Regression analysis showed Nd and Sm titrations fit very well to a 2 species model (free MC and 1:1 adduct (**Ln-MC**)Muc), indeed consistent with calorimetric data which excluded the formation of 2:1 (**Ln-MC**)$_2$Muc adducts (Figures S11 and S12). On the other hand, a very good fit of data for the titration of Eu was obtained by considering the presence of all three MC species: free metallacrown, 1:1 and 2:1 species (Figure 3). The exclusion of the 2:1 species did not provide a good fit to the experimental data (details in Supporting Information).

The consistency of this model with theoretical expectations was analyzed according to a Stokes-Einstein model that assumes spherical particles, with volume, V, proportional to the cube of the van der Waals radius, r, according to $V = \frac{4}{3}\pi r^3$.

For a complex that dimerizes, the van der Waals volume is presumed to double, so that $V_{dimer} = 2(V_{monomer}) \propto r_{dimer}{}^3$. This corresponds to an increase of the mean van der Waals radius by a factor equal to $\sqrt[3]{2} = 1.26$, with a corresponding decrease in diffusion coefficient, D, and therefore also D', by a factor of 1.26. Our least squares analysis of the **Eu-MC** system indicated that $D'_{2:1}$ is lower than D'_{MC} by a factor of 1.14. The difference from the theoretical value is, therefore, a factor of just 0.12 corresponding to a difference in radius of approximately 0.7 Å, which is less than a solvation shell around the MC dimer. The deviation from theoretical behavior may be accounted for by structural aspects, such as solvent effects (NMR was performed in 50% MeOD solution), which may alter the side chain interactions, or deviation from sphericity of MC particles. If the latter explanation is considered, measurements from crystal structures[4a,c] show that the monomer could be considered more oblate (Scheme 1B), which could lead to more resistance to diffusion, and that the dimer is more spherical (Scheme 1D), with the effect that the dimer would diffuse faster than expected.

Analysis of lanthanide trend

Plotting the present work's log K stability constants against lanthanide radius (Figure 4A) for Sm^{3+} through Ho^{3+} (Figure S13, all examined **Ln-MCs**), we notice a correlation between the first and second complexation events. If the binding constant of the first step (K_1, referring to **MC** + Muc⇄(**MC**)Muc) is weak, the binding constant of the second step (K_2, indicating **MC** + (**MC**)Muc⇄(**MC**)$_2$Muc) is stronger and compartment formation is observed.

However, in those cases where K_1 is large, such as that of Sm and Nd, the second step was not detected. Furthermore, we notice the plot of the binding constants exhibits a pattern of two opposing V shapes, with Gd as the apex and nadir of each. If we continue the trend down from the K_2 of Gd and Dy, Ho's second binding constant would be quite close to its first, such that the second binding event may be disfavored due to the high stability of the 1:1 (**Ln-MC**)Muc complex. A similar observation can be made for Sm^{3+}, where the theoretical K_2 point would be notably close to its K_1.

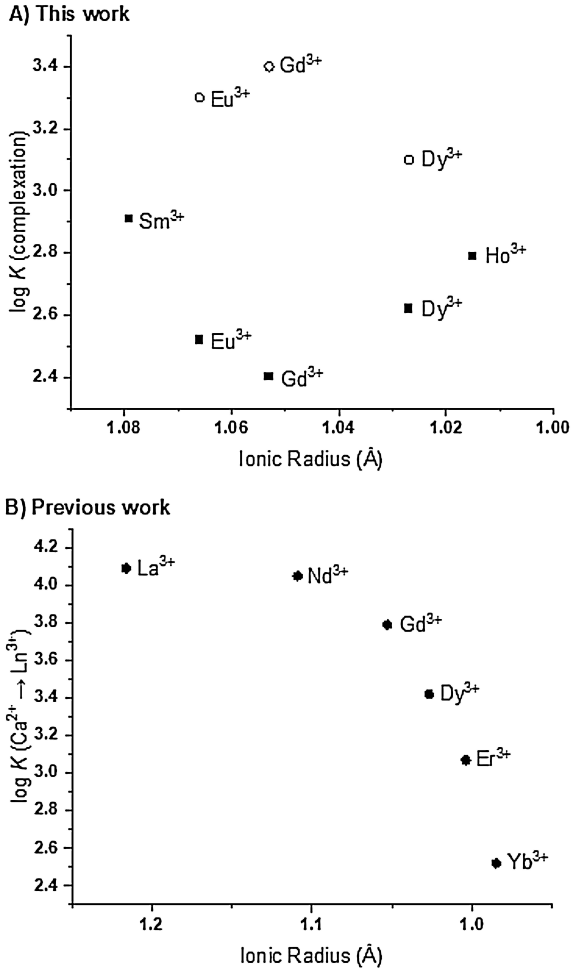

Figure 4. A) Stability constants for 1st and 2nd complexation events of muconate guest with MC host according to lanthanide species ionic radius.[6] Selected lanthanides Sm^{3+} through Ho^{3+} with ionic radii of 8-coordinate species. Black squares: K_1 values to describe the equilibrium **MC** + Muc ⇄ (**MC**)Muc; Open circles: K_2 values for **MC** + (**MC**)Muc ⇄ (**MC**)$_2$Muc. B) Previously published stability constants of Ln^{3+} substitution for Ca^{2+} in the 15-MC-5 motif (99:1 MeOH:H_2O; ligand is tryptophan hydroxamic acid).[8a]

Unfortunately, we cannot determine whether this thermodynamic observation is a cause or an effect of compartment formation. However, to explain the observed lanthanide trend, we considered the crystallographic structures and thermodynamic data in the literature. The larger lanthanides are known to have greater affinity for the 15-MC-5 macrocycle (Figure 4B)[8a] and are thus highly stable structures in their monomeric form. In crystal structures, La^{3+} and Nd^{3+} both have been found to favor lying out of the MC plane towards the hydrophilic face in the absence of carboxylate guests, whereas smaller lanthanides have more frequently been found to lie toward the hydrophobic face or fit into the plane of the MC ring.[7] When a guest molecule is introduced, crystal structures with La^{3+} have often been shown to bind guests on the hydrophilic face in addition to examples with binding on the hydrophobic face with significant variation in binding modes (for example, bidentate to La^{3+}, bridging La^{3+} and ring Cu^{2+}).[3b,e,4a,b] As a consequence of the protrusion of the larger lanthanides, we believe it is more difficult for guest binding to achieve the appropriate orientation to bridge the hydrophobic faces of two MCs to form the (**Ln**-**MC**)$_2$Muc structure.

On the other hand, the weak propensity for Ho to yield the (**Ln**-**MC**)$_2$Muc species indicates that an opposing trend takes over for the latter end of the lanthanide series. The size mismatch of the heavier Ln's within the 15-MC-5 ring is reflected in their lower stability constants (Figure 4B). The smaller lanthanides do not accommodate as well the Ln–O distance required to bind effectively to the five metallacrown ring oxygen atoms. Therefore, ions such as Ho^{3+} must stay nearly within the plane of the oxygen atoms to form a stable host complex. At the same time, crystal structures with smaller Ln's typically are consistent with guest binding in the orientation to bridge the hydrophobic faces of two MCs.[3b,e,4a,c] However, bridging a dicarboxylate to form (**MC**)$_2$Muc from (**MC**)Muc and another **MC** forces the lanthanide ion to be more displaced from the 15-MC-5 ring, which weakens the stability of the host. Therefore, the system favors the 1:1 complex for the later Ln's due to the low binding constant of the Ln within the ring, despite the presumably favorable orientation of the guest and high Lewis acidity of the central lanthanide.

Size dependency of rare earth-complex formation has been well-documented, especially in rare earth element separations, with examples ranging from tripodal ligands with a size-sensitive lanthanide binding aperture and monomer/dimer equilibrium[15] to lanthanide-dependent self-assembly of varied polyhedra.[16] Most of these examples, as well as bioinorganic examples of lanthanide-containing bacterial proteins,[17] derive selectivity primarily from size and steric based considerations discriminating best between early and late lanthanides with systematic increasing or decreasing trends in binding constant. Much less common are compounds that exhibit their highest selectivity for intermediate lanthanides, including Ln^{3+}(OBETA) reported by Platas-Iglesias and Botta,[18] and Ln^{3+}(TCMC) described by Morrow.[19] Notably, while the stability of Ln^{3+} complexation within the 15-MC-5 macrocycle has previously been shown to follow a systematic decrease across the lanthanide series (Figure 4B),[8a] the phenomenon we have described with respect to the host-guest chemistry for compartment formation of MCs with a dicarboxylate guest is only observed for intermediate lanthanides. The narrow range of lanthanides involved in the MC dimerization phenomenon must be achieved through a balance of Ln size and favorable molecular interactions to bind a second MC.

Conclusion

The calorimetric results in combination with the NMR data detailed above converge to provide compelling evidence from two experimentally distinct and independent techniques that the identity of the lanthanide affects the dimerization phenomenon. **Ln**-**MCs** with Eu, Gd, and Dy are able to dimerize in the presence of a dicarboxylate guest to form 2:1 (**Ln**-**MC**)$_2$Muc species in equilibrium with 1:1 (**Ln**-**MC**)Muc species and free

MC monomer, whereas larger lanthanides such as La, Nd, Sm, and smaller ones like Ho can only form the (**Ln**-**MC**)Muc species in equilibrium with the monomer. Based on the ΔH values, that to some extent quantitate the favorable intramolecular interactions determining the formation of the molecular container, the Gd-based metallacrown is the one in which the π-π interaction between the phenyl substituents of the two converging halves of the compartment is maximized. While most Ln-containing systems follow systematic increasing or decreasing trends in the equilibrium constant according to the size of the Ln, there are relatively few examples where the stability peaks half-way through the lanthanide series. Furthermore, this is the first example where the identity of the lanthanide has consequences for host-guest supramolecular assembly.

In the MC supramolecular system, the size of the lanthanide was proven to play a critical role, which has implications for the development of lanthanide-containing catalytic systems and informs our basic understanding of the complex characteristics of lanthanides in coordination complexes.

Experimental Section

Materials

All reagents were obtained from commercial sources and used as received unless specified. Ln^{III}(15-MC-$_{Cu^{II}N(L\text{-}pheHA)}$-5)$^{3+}$ complexes were prepared based on literature procedure as previously described.[7]

Example synthesis of Ln^{III}(15-MC-$_{Cu^{II}N(L\text{-}pheHA)}$-5)$^{3+}$

L-phenylalanine hydroxamic acid (*L*-pheHA) (1.0 mmol), Cu(OAc)$_2\cdot H_2O$ (1.0 mmol) and Ln(NO$_3$)$_3\cdot 6H_2O$ (0.20 mmol) were stirred in 20 mL of H_2O plus 2 mL MeOH for 2 h. The solution was gravity filtered to remove green precipitate and left for slow evaporation (~1 month) to yield deep blue-purple crystals.

Additional reagents for calorimetry

Muconate (Muc) was of the highest purity commercially available (98%, Sigma Aldrich) and was used as received. KOH solutions (Merck, Titrisol Normex), used to have Muc in its fully deprotonated form, were standardized by titration with potassium hydrogen phthalate. High purity water (Millipore, Milli-Q Element A 10 ultrapure water) and grade A glassware were employed throughout.

Additional reagents for NMR

Trans-trans muconic acid (Acros) used for NMR studies was recrystallized from hot THF. Dipotassium muconate (Muc) was prepared by neutralizing the recrystallized muconic acid in water with potassium hydroxide and precipitating the solid with acetone. The solid was collected by vacuum filtration, rinsed with ether, and dried under vacuum.

Isothermal titration calorimetry: Preliminarily solubility tests were carried out to define the optimal experimental conditions for ITC measurements. All **Ln**-**MC**s are soluble (~1 mM) in water at pH 7.2, the pH value selected to have Muc in the dianionc form. However, potentiometric measurements indicated that pH slightly changes over 3–4 h; thus a suitable buffer (50 mM MOPS) was used in all ITC experiments.

ITC titrations were carried out at 25 °C using two isothermal titration calorimeters (Nano-ITC, TA Instruments) equipped with a 100 μL injection syringe. The reaction mixture in the sample cell was stirred at 250 rpm during the titrations. All solutions were softly degassed under vacuum for about 15 min before each experiment. The calorimeters were calibrated chemically by a test HCl/TRIS reaction according to the procedure previously described.[10a] The instruments were also double checked through an electrical calibration.

ITC measurements were carried out by titrating aqueous solution of Muc into a **Ln**-**MC** solution; both **Ln**-**MC** and Muc were dissolved in 50 mM MOPS buffer (pH 7.2) to minimize any contribution from the interaction of either the guest or the **MC**s with the proton.

The equilibrium between the 1:1 ((**Ln**–**MC**)Muc) and 2:1 ((**Ln**-**MC**)$_2$Muc) species is shifted towards the compartment in the first region of the calorimetric curve, that is in the presence of excess **Ln**-**MC**, and consequently two sets of experiments were specifically designed for this purpose. Full scan titrations (C_{Muc} = 38–42 mM, $C_{Ln\text{-}MC}$ = 0.4–0.5 mM, Muc/**MC** ratio up to 8) were run to define the 1:1 species, whereas expanded titrations (C_{Muc} = 4–6 mM, $C_{Ln\text{-}MC}$ = 0.9–1.1 mM, Muc/**MC** ratio up to 0.4) were run to better detect the 2:1 ((**Ln**-**MC**)$_2$Muc) complex that, when existing, is fully formed in the very first points of the full scan experiment.

The heats of dilution were determined in separate blank experiments by titrating solutions of Muc (in MOPS) into a solution containing MOPS only. An example of the power curve for a dilution experiment is included in Figure S4. 6–7 independent experiments were usually run for each system to collect a proper number of data points to satisfactorily analyse both the first and last portion of the calorimetric curve.[10a] The net heats of reaction, obtained by subtracting the heat from the blank experiments, were handled by HypCal, a software able to refine both stability constant and enthalpy change values and to simultaneously treat data from multiple titrations.[11] The two sets of experiments (full scan and expanded titrations) were refined together to obtain the final parameters.

NMR experiments

One and two dimensional ^{1}H NMR were performed on a 400 MHz spectrometer (Varian MR400) equipped with Varian 5 mm PFG AutoX Dual Broadband probe (T_1 inversion recovery) or a 500 MHz spectrometer (Varian V NMRS) equipped with a Varian 5 mm PFG OneNMR Probe (PGSE DOSY experiments).

One dimensional ^{1}H NMR spectra of the **Ln**-**MC**s (Figure S5) were taken for samples of 2 mM **Ln**-**MC** (excepting **Gd**-**MC**, which was 6 mM) in 100 mM MOPS buffer in D_2O (pD 7.2 ± 0.1, pD corrected from pH reading for D_2O[20]). Using these samples for the T_1 inversion recovery experiments, a standard two-pulse sequence was used using 15 delay time values (τ) ranging from 0.001 s to 0.3 s between the 180° and 90° pulses and a relaxation delay of 1.2 s, except in the case of Gd in which case τ values range from 0.0001 s to 0.3 s.

The pulsed gradient spin echo (PGSE) experiment used a standard double stimulated echo pulse sequence with a convection compensation and a duration of rectangular gradient pulses, δ, of 2.2 ms (Sm, Nd) or 3.2 ms (Eu), a delay between gradient pulses, Δ, of 45 ms (Eu), 50 or 70 ms (Sm), or 90 ms (Nd), and constant

temperature (25 ± 0.3 °C). For the PGSE, fifteen spectra were collected with varying gradient strength, *G*, from 2.4 to 59.6 G/cm with relaxation delay, d_1, of 0.5 s (Sm, Nd) or 0.2 s (Eu) and acquisition time of 3.5 s (Sm) or 2.0 s (Nd, Eu).

NMR titrations were performed in triplicate and carried out in 1:1 MeOD:D_2O buffer (100 mM MOPS, pD 7.2 ± 0.15, pD corrected from pH reading for D_2O,[20] prior to dilution with MeOD) with DMSO used as an internal standard. Deuterated methanol was used to avoid precipitation at the mM level concentrations that were necessary for NMR. An exception is for 6 mM **Eu-MC** - sorbate titration: only two PGSE experiments were performed for the points at 0.58 equiv. and 1 equiv.; only 10 G^2 values were used for one of the experiments at 0.83 equiv. NMR Spectra processing and analysis, including fit of T_1, was performed using MestReNova 11.0.2 software. All other least square regression analyses were performed using SPSS Statistics 26.0 software.

A detailed account of the mathematical treatment for analyzing the NMR titrations is included in the Supporting Information, including a new treatment for translating the error of the measured diffusion coefficient into corresponding error for hydrodynamic radius.

Acknowledgements

MIUR (PRIN 2015–2015MP34H3) and University of Catania (Piano della Ricerca d'Ateneo 2016-18, linea 2 and PIACERI 2020–22, linea d'intervento 2) are acknowledged for partial financial support (C.S. & G.A.). The National Science Foundation (NSF) is acknoweledged under the grant CHE-1664964 (V.L.P.). M.T. has benefited from the equipment and framework of the COMP-HUB Initiative, funded by the "Departments of Excellence" program of the Italian Ministry for Education, University and Research (MIUR, 2018-2022). The contribution of C.S., G.A. and M.T. was carried out within the framework of COST Action CA18202, NECTAR-Network for Equilibria and Chemical Thermodynamics Advanced Research, supported by COST (European Cooperation in Science and Technology).

Conflict of Interest

The authors declare no conflict of interest.

Keywords: calorimetry · diffusion ordered NMR · host-guest systems · lanthanides · metallacrowns

[1] C. J. Brown, F. D. Toste, R. G. Bergman, K. N. Raymond, *Chem. Rev.* **2015**, *115*, 3012–3035.
[2] a) V. L. Pecoraro, A. J. Stemmler, B. R. Gibney, J. J. Bodwin, H. Wang, J. W. Kampf, A. Barwinski, in *Prog. Inorg. Chem.* (Ed.: K. D. Karlin), John Wiley & Sons, Inc., New York, **1996**, pp. 83–177; b) G. Mezei, C. M. Zaleski, V. L. Pecoraro, *Chem. Rev.* **2007**, *107*, 4933–5003; c) J. C. Lutter, C. M. Zaleski, V. L. Pecoraro, in *Adv. Inorg. Chem., Vol. 71* (Eds.: R. van Eldik, R. Puchta), Academic Press, Cambridge, MA, **2018**, pp. 177–246.
[3] a) A. D. Cutland, R. G. Malkani, J. W. Kampf, V. L. Pecoraro, *Angew. Chem. Int. Ed.* **2000**, *39*, 2689–2691; *Angew. Chem.* **2000**, *112*, 2801–1803; b) C. S. Lim, J. W. Kampf, V. L. Pecoraro, *Inorg. Chem.* **2009**, *48*, 5224–5233; c) C. S. Lim, J. Jankolovits, P. Zhao, J. W. Kampf, V. L. Pecoraro, *Inorg. Chem.* **2011**, *50*, 4832–4841; d) M. Tegoni, M. Tropiano, L. Marchio, *Dalton Trans.* **2009**, 6705–6708; e) J. Jankolovits, J. W. Kampf, S. Maldonado, V. L. Pecoraro, *Chem. Eur. J.* **2010**, *16*, 6786–6796.
[4] a) A. D. Cutland, J. A. Halfen, J. W. Kampf, V. L. Pecoraro, *J. Am. Chem. Soc.* **2001**, *123*, 6211–6212; b) J. Jankolovits, C. S. Lim, G. Mezei, J. W. Kampf, V. L. Pecoraro, *Inorg. Chem.* **2012**, *51*, 4527–4538; c) C. S. Lim, A. C. V. Noord, J. W. Kampf, V. L. Pecoraro, *Eur. J. Inorg. Chem.* **2007**, *2007*, 1347–1350.
[5] C. Sgarlata, A. Giuffrida, E. R. Trivedi, V. L. Pecoraro, G. Arena, *Inorg. Chem.* **2017**, *56*, 4771–4774.
[6] R. D. Shannon, *Acta Crystallogr. Sect. A* **1976**, *32*, 751–767.
[7] C. M. Zaleski, C.-S. Lim, A. D. Cutland-Van Noord, J. W. Kampf, V. L. Pecoraro, *Inorg. Chem.* **2011**, *50*, 7707–7717.
[8] a) M. Tegoni, M. Furlotti, M. Tropiano, C. S. Lim, V. L. Pecoraro, *Inorg. Chem.* **2010**, *49*, 5190–5201; b) C.-S. Lim, M. Tegoni, T. Jakusch, J. W. Kampf, V. L. Pecoraro, *Inorg. Chem.* **2012**, *51*, 11533–11540.
[9] a) C. Sgarlata, J. S. Mugridge, M. D. Pluth, B. E. F. Tiedemann, V. Zito, G. Arena, K. N. Raymond, *J. Am. Chem. Soc.* **2010**, *132*, 1005–1009; b) C. Bonaccorso, G. Brancatelli, G. Forte, G. Arena, S. Geremia, D. Sciotto, C. Sgarlata, *RSC Adv.* **2014**, *4*, 53575–53587; c) C. Bonaccorso, A. Ciadamidaro, V. Zito, C. Sgarlata, D. Sciotto, G. Arena, *Thermochim. Acta* **2012**, *530*, 107–115; d) C. Bonaccorso, C. Sgarlata, G. Grasso, V. Zito, D. Sciotto, G. Arena, *Chem. Commun.* **2011**, *47*, 6117–6119; e) C. Sgarlata, C. Bonaccorso, F. G. Gulino, V. Zito, G. Arena, D. Sciotto, *Tetrahedron Lett.* **2009**, *50*, 1610–1613; f) G. Arena, C. Sgarlata, in *Comprehensive Supramolecular Chemistry II, Vol. 2* (Ed.: J. L. Atwood), Elsevier, Oxford, **2017**, pp. 213–237.
[10] a) C. Sgarlata, V. Zito, G. Arena, *Anal. Bioanal. Chem.* **2013**, *405*, 1085–1094; b) L. S. Mizoue, J. Tellinghuisen, *Anal. Biochem.* **2004**, *326*, 125–127.
[11] G. Arena, P. Gans, C. Sgarlata, *Anal. Bioanal. Chem.* **2016**, *408*, 6413–6422.
[12] C. Atzeri, V. Marzaroli, M. Quaretti, J. R. Travis, L. Di Bari, C. M. Zaleski, M. Tegoni, *Inorg. Chem.* **2017**, *56*, 8257–8269.
[13] I. Bertini, C. Luchinat, *Coord. Chem. Rev.* **1996**, *150*, 77–110.
[14] Y. Cohen, L. Avram, L. Frish, *Angew. Chem. Int. Ed.* **2005**, *44*, 520–554; *Angew. Chem.* **2005**, *117*, 524–560.
[15] a) J. A. Bogart, B. E. Cole, M. A. Boreen, C. A. Lippincott, B. C. Manor, P. J. Carroll, E. J. Schelter, *Proc. Natl. Acad. Sci. USA* **2016**, *113*, 14887 LP-14892; b) B. E. Cole, I. B. Falcones, T. Cheisson, B. C. Manor, P. J. Carroll, E. J. Schelter, *Chem. Commun.* **2018**, *54*, 10276–10279.
[16] a) X.-Z. Li, L.-P. Zhou, L.-L. Yan, Y.-M. Dong, Z.-L. Bai, X.-Q. Sun, J. Diwu, S. Wang, J.-C. Bünzli, Q.-F. Sun, *Nat. Commun.* **2018**, *9*, 547–547; b) X.-Z. Li, L.-P. Zhou, S.-J. Hu, L.-X. Cai, X.-Q. Guo, Z. Wang, Q.-F. Sun, *Chem. Commun.* **2020**, *56*, 4416–4419.
[17] J. A. Cotruvo Jr, *ACS Cent. Sci.* **2019**, *5*, 1496–1506.
[18] a) Z. Baranyai, M. Botta, M. Fekete, G. B. Giovenzana, R. Negri, L. Tei, C. Platas-Iglesias, *Chem. Eur. J.* **2012**, *18*, 7680–7685; b) R. Negri, Z. Baranyai, L. Tei, G. B. Giovenzana, C. Platas-Iglesias, A. C. Bényei, J. Bodnár, A. Vágner, M. Botta, *Inorg. Chem.* **2014**, *53*, 12499–12511.
[19] D. A. Voss, E. R. Farquhar, W. D. Horrocks, J. R. Morrow, *Inorg. Chim. Acta* **2004**, *357*, 859–863.
[20] A. K. Covington, M. Paabo, R. A. Robinson, R. G. Bates, *Anal. Chem.* **1968**, *40*, 700–706.

Manuscript received: September 8, 2021
Accepted manuscript online: October 12, 2021
Version of record online: November 5, 2021

